machines

MDPI

Article

"Rigid Press Device (RPD)" for Robotic Stack Drilling in Aircraft Assembly

Takehiro Hayasaka *, Ryuto Sawabe, Kyungki Lee and Eiji Shamoto

Graduate School of Engineering, Nagoya University, Furo-cho, Chikusa-ku, Nagoya 464-8603, Japan
* Correspondence: hayasaka.takehiro.g6@f.mail.nagoya-u.ac.jp

Abstract

In this paper, a Rigid Press Device (RPD) is proposed for robotic stack drilling in aircraft assembly. Although robots have widened their applicability, robot machining is rarely applied, mainly due to their low stiffness. Meanwhile, the interlayer gap problem occurs during the stack drilling of plates, e.g., chips entering the interlayer gap caused by the drilling thrust force. Although systems such as a pressure foot and/or a dedicated end effector may be utilized for the latter problem, they are generally not designed to increase rigidity. To solve these problems simultaneously, a Rigid Press Device is developed, where pressing is intended to eliminate the gap and its small closed compliance loop is intended to increase the rigidity of the machining system. The effectiveness of the developed device is clarified through the hammering of the system and drilling experiments of a two-layer aluminum stack mounted on a robot-imitating compliant structure, where the rigidity-increase effect (e.g., an 88% decrease in the magnitude of the dynamic compliance) is confirmed; the interlayer chip/burr and vibration are suppressed (e.g., the suppression of chatter vibration of 870 μm amplitude); and the hole accuracy is increased.

Keywords: drilling; robot; stacks; compliance loop; Rigid Press Device (RPD); interlayer gap; chatter vibration; forced vibration; accuracy

1. Introduction

The industrial need for robot machining has increased greatly in the recent years [1–3]. Although robots are widely used for various operations such as handling and assembly, their usage for machining is limited. A major reason for this limitation is the low rigidity of the robot [1–3], which causes many problems such as chatter [4] and low precision [5–7] in various machining operations, e.g., drilling and milling. Therefore, it is crucial to tackle these problems to further increase the implementation of robots in various industries.

One field that has shown increased interest in robot machining is aircraft manufacturing/assembly. For example, The Boeing Company conducted a project called FAUB (fuselage automated upright build), where the manual drilling and riveting of the fuselage were attempted to be replaced by robot operations [8]. During the assembly of fuselages, holes were machined on stacks of multiple plates at once rather than preliminarily on each plate, mainly as a means of reducing the misalignment of the holes [9]. Although there are many ways to machine these holes, drilling is still the most common method utilized in practice [8]. At present, this drilling is conducted either by an extremely large automatic riveting machine [9] or by hand in the shop. However, the former method requires a large space and incurs high costs, and the latter method hinders automation and increases labor costs. These are the reasons that robots are being introduced into practice, as they are

Check for updates

Academic Editor: Kourosh Tatar

Received: 17 September 2026
Revised: 7 October 2026
Accepted: 8 October 2026
Published: 16 October 2026

Copyright: © 2026 by the authors. Licensee MDPI, Basel, Switzerland. This article is an open access article distributed under the terms and conditions of the Creative Commons Attribution (CC BY) license.

less costly and require less installation space than riveting machines, and they also assist automation compared with manual operation. Nevertheless, robot machining is rarely applied to this field in practice, largely because of the low rigidity of both the robot and the relatively thin fuselage structure. More specifically, the compliance loop of the system (which is composed of the robot and fuselage structure) is large and prone to vibration, as shown in Figure 1a. Note that large robots may be capable of this machining, but they lack the practicality of riveting machines.

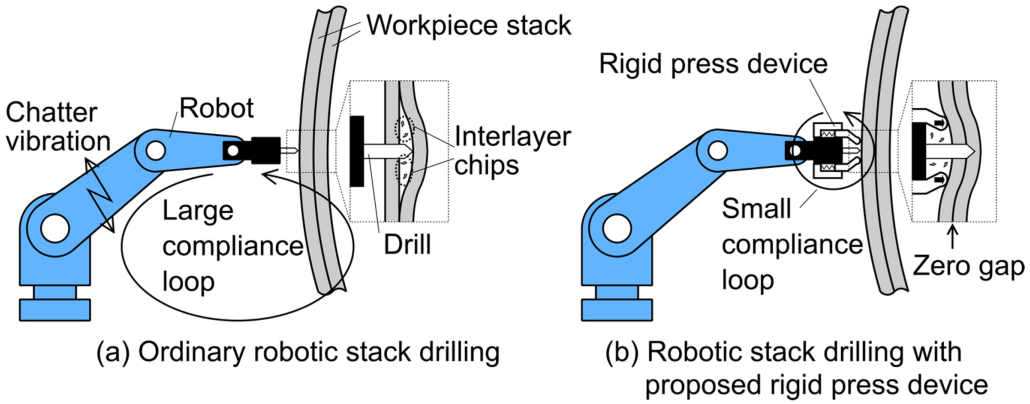


Figure 1. Problems in robotic stack drilling and the proposed solution.

Meanwhile, a particular problem arises from chips formed during stack drilling. During drilling, the thrust (feed) force causes the plates to deform elastically. After the top plate is drilled completely, its deformation is released, and an interlayer gap forms between the top and bottom plates because the bottom plate is still being pushed by the drill [10,11]. As the cutting continues, the chips formed in the drilling of the bottom plate enter the gap, as shown in Figure 1a. Therefore, the plates need to be disassembled for the removal of the chips, and then the plates must be reassembled [9]; this causes the manufacturing cost to increase. Burrs formed in the interlayer gap cause a similar problem during drilling stacks.

Many attempts have been made to solve these problems. Specific robot postures may have relatively higher rigidity [12,13]. However, low-rigidity postures are difficult to avoid when manufacturing large parts. As for the interlayer gap problem, step drills and other drill geometries have been introduced to decrease or disperse the thrust force and thereby reduce the gap [14,15], but they cannot eliminate the gap. From another perspective, pressure feet are often used to push the plates from the top [16,17], but they operate independently of robots. Similarly, the idea of pushing the plates using a pressure foot installed in specially designed robot end-effectors has been realized [18–20], but these studies do not focus on its effect on robot/fuselage rigidity and dynamic stability; thus, this effect remains unclear. Moreover, existing pressure feet and end-effectors are not designed with a focus on the compliance loop of the system. For example, the pressure feet and/or end-effectors utilized in [21–23] are designed to apply pressure, but the pressure-foot structure does not always have a rigid/sturdy structure, thereby hindering the loop size to be small.

Based on this background, a robotic stack-drilling method that can simultaneously suppress the interlayer gap and problems associated with low rigidity, such as chatter, is required to improve the machining capability of robots.

In this research, a Rigid Press Device (RPD) is proposed and developed for robotic stack drilling; it can suppress the interlayer gap and low-rigidity problems simultaneously, as shown in Figure 1b. This drilling is hereinafter called RPD-drilling in this study. By pressing the plates from the top, the interlayer gap can be eliminated. In addition, the high-rigidity structure of the press device forms a small closed compliance loop of the machining system owing to the static friction by the pressing force, that is, the rigidity of the system can be

increased even when the dynamics of the low-rigidity robot and thin plates are included. The main contributions of this research are summarized as follows:

1. The RPD and RPD-drilling are proposed for the advancement of robotic stack drilling.
2. The RPD is designed with a focus on a small closed compliance loop and pressing force demands.
3. The RPD's rigidity-increasing effect is investigated through hammering tests.
4. The suppression of interlayer chips/burr, suppression of chatter/forced vibration, and improvement of hole accuracy by the RPD are investigated through drilling tests.

2. Design and Effect of the Proposed Rigid Press Device

2.1. Device Design

The designed RPD is shown in Figure 2. Beginning from the top, the device is composed of base parts (C50, ISO), radial-direction high-rigidity parts (140 × 90 × 35 mm, C50, ISO), springs (diameter: 25 mm, length: 75 mm, stiffness: k_s = 13.1 N/mm for each, SWF-25-75, MISUMI Corp (Chiyoda, Japan)), linear bushes (50 mm × 54 mm × 41 mm, LHBBN20L, MISUMI Corp.), shafts (diameter: 20 mm, length: 120 mm, 683-17, ISO), a ring plate (thickness: 5 mm, C50, ISO), and press points (C50, ISO). In this paper, two press points are designed to press the workpiece, and the ring plate is designed so that these two points act nearly simultaneously on the workpiece by guiding it through a pair of shafts and linear bushes. The height difference between the tip of the drill and the press points is adjusted to apply sufficient pressing force before drilling of the top plate begins, in order to withstand any lateral displacement by friction at the press points; the small closed compliance loop is formed owing to the rigidity of the proposed device. To serve as a highly rigid structure, the parts supporting the moving components—i.e., springs, linear bushes, and ring plates in this paper—are designed to be rigid, i.e., thick in radial directions. This design feature keeps the closed compliance loop small. Note that static lateral force/displacement should generally not occur in drilling since the multiple teeth perform balanced cutting, and the proposed RPD should suppress chatter, resulting in no dynamic force/displacement. In addition, it is also adjusted to apply sufficient pressing force before the drilling of the bottom plate begins in order to eliminate the interlayer gap; generation of interlayer chips/burr can thus be suppressed. Thanks to this passive pressing of the plates, the device is made compact.

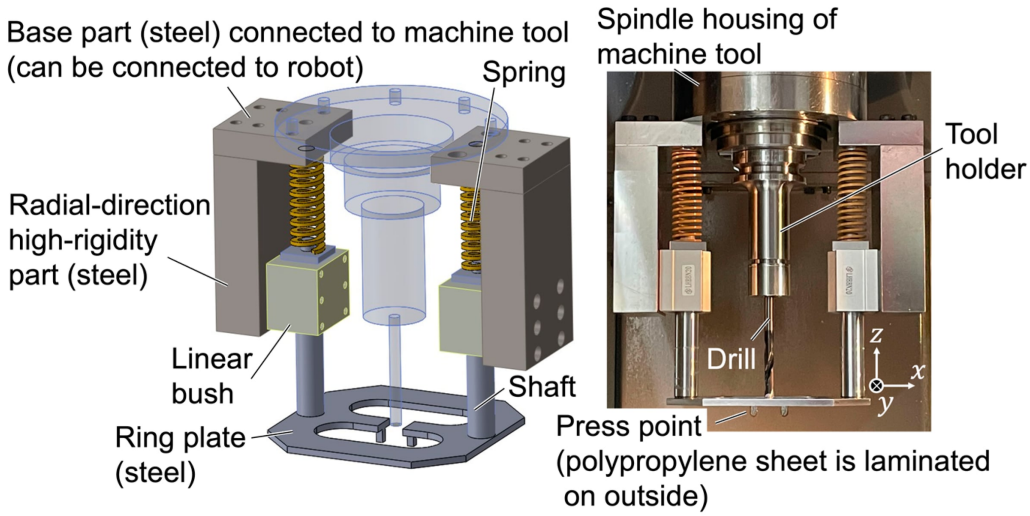


Figure 2. Three-dimensional CAD drawing and photograph of proposed RPD.

Because a small closed compliance loop is formed using the RPD during the drilling, the rigidity of the drilling system can be greatly increased, as shown in Figure 1b. Note that the rigidity in the z (thrust) direction is not designed to increase much, i.e., it is increased by springs, but if necessary, it can be increased by eliminating the springs and using a drilling unit with a separate feed mechanism so that the positions of the drill and the press points are controlled separately. Note also that as the press points contact the aluminum workpiece directly, they are laminated with thin polypropylene sheets of 0.2 mm thickness so that the plastic deformation of the aluminum surface is suppressed.

Another important part of the design is the pressing force. This force must be sufficiently large to eliminate the interlayer gap. Considering the compliance of the top and bottom plates G_t and G_b, respectively, and the initial gap between the plates g_{init}, the pressing force F_p and the thrust force in drilling of the bottom plate F_d must satisfy the following relationship:

$$F_p > (G_b F_d + g_{init})/G_t \quad (1)$$

Note that $G_b F_d$ is the deflection of the bottom plate by the thrust force, $G_b F_d + g_{init}$ is the interlayer gap, and $G_t F_p$ is the deflection of the top plate by the pressing force. Note also that the initial gap can occur due to the shape error of the workpiece and distortion by clamping. For the case in this paper, the two plates have the same specifications (i.e., the same thickness, width, and nearly same boundary conditions). Therefore, $G_t = G_b$, and it is assumed that the initial gap is zero; hence, the pressing force simply has to be larger than the drilling force ($F_p > F_d$) before the drilling of the bottom plate begins. Note that FEM simulations of the structure may be conducted to identify factors of compliance G_t and G_b in a precise manner. The pressing force can be adjusted by the stiffness of the springs and the height difference between the tip of the drill and the press points. More specifically, let z_d and z_p denote the original height (without pressing) of the drill and the press points, respectively, where z is smaller if it is closer to the workpiece, and let t_t and t_p denote the thicknesses of the top plate and bottom plate of the stack, respectively. N_s denotes the number of springs. The pressing force at the beginning of the drilling of the top plate can be calculated using $N_s k_s(z_d - z_p)$. The friction incurred by this force must be large enough to withstand the lateral force/displacement and maintain the small closed compliance loop. Similarly, the pressing force at the beginning of the drilling of the bottom plate can be calculated by $F_p = N_s k_s(z_d - z_p + t_t)$, and this force must satisfy Equation (1) so that the interlayer gap is suppressed. Note that the pressing force at the end of the drilling of the bottom plate can be calculated using $N_s k_s(z_d - z_p + t_t + t_b)$, and the sum of this force and the thrust force should be smaller than the maximum allowable force of the machine structure, e.g., the payload of the robot. With the selected springs in this paper, the difference between the tip of the drill and the press points is adjusted to 18.7 mm, i.e., $z_d = 0$ and $z_p = -18.7$ mm, which results in a pressing force of roughly 600 N when the drilling of the bottom plate begins, i.e., after pressing of 22.7 mm including the thickness of the top plate. Note that a margin of around 100 N and a drilling thrust force of the bottom plate of around 500 N are set in the experiments, since there are some uncertainties in the experiments, e.g., the initial interlayer gap.

2.2. Rigidity-Increasing Effect of the Device

The dynamic loop compliance of the drilling system is measured to confirm the rigidity-increasing (compliance-decreasing) effect of the proposed press device. In this paper, the compliance of a robot is imitated for the compliance loop of the aircraft assembly. A low-rigidity structure composed of four rubber springs (with a stiffness of 70 N/mm for each, VD3-2530M6, Imao Corp (Seki, Japan)) and a mass part (C50, ISO) is developed. Its photograph is shown in Figure 3. The compliance of robots measured in conventional

studies [4,24] is used as a reference for the maximum magnitude of the dynamic compliance and natural frequencies of robotic modes, and the structure is designed so that the former is several tens of micrometers/N and the latter is several tens of Hz. The compliance is measured in two settings, where one is without any pressing and the other is with pressing by the developed device at a pressing force of 500 N. The setup with pressing is shown in Figure 4. Accelerometers (3713F1130G, PCB Piezotronics, Inc. (Depew, NY, USA)) are set on the tool side and the low-rigidity structure side, and two compliances are measured using a hammer (086C01, PCB Piezotronics, Inc.) where one is with the hammering of the tool side, and the other is with the hammering of the low-rigidity structure side. For each compliance, the relative displacement is obtained from the difference between the accelerometers and used to calculate each relative compliance. More specifically, let A_{tt} and A_{lt} denote the Fourier-transformed vibration accelerations of the tool side and the low-rigidity structure side when the tool is hammered, respectively; let A_{tl} and A_{ll} denote the Fourier-transformed vibration accelerations of the tool side and the low-rigidity structure side when the low-rigidity structure is hammered, respectively; and let F_t and F_l denote the Fourier-transformed forces measured when the tool and the low-rigidity structure are hammered, respectively. The relative accelerances obtained by hammering the tool and the low-rigidity structure are then calculated by $(A_{tt} - A_{lt})/F_t$ and $(A_{ll} - A_{tl})/F_l$, respectively. Note that all accelerations and forces are defined using a common global coordinate system. Then, the two relative accelerances are converted into relative compliances by double integration, i.e., dividing by $-\omega^2$ where ω is the angular frequency, and the resulting compliances are added to obtain the loop compliance. The direct components of the measured loop compliances are shown in Figure 5. The grey lines show the compliances without pressing, and the black lines show those with pressing. Note that only a single pressing force and a single compliance (posture in robots) have been tested in these experiments, but the former should not affect the stiffness of the system, as only the force changes and the system remains unchanged. However, note also that this force may change the contact state of various components, thereby slightly affecting the damping/stiffness characteristics. As shown, the maximum magnitudes of the dynamic compliances of those without pressing are around 74, 75, and 13 μm/N in the x, y, and z directions, respectively, and the resonant frequencies are around 21, 21, and 47 Hz, respectively. These are comparable to those of the robots in the literature, where former values are even larger than them. For example, a maximum compliance of around 25 μm/N is observed in [4] and around 50 μm/N is observed in [24]. Their resonant frequencies are also comparable, being around 13 to 25 Hz in [4] and around 12 to 24 Hz in [24]. Therefore, these results suggest that the robot's compliance is appropriately imitated. For reference, the modal parameters (mass, damping ratio, and spring constant) are summarized in Table 1, and it can be observed that the damping ratio is also similar to results in the existing literature, e.g., 1.24% to 3.05% in [4]. Regarding the proposed method, the magnitude of the loop compliance decreases greatly with the developed press device, with a maximum decrease of 88% in the x direction. As shown in Table 1, not only the increase of the rigidity (spring constant), but also the increase of the damping ratio contributed to the decrease of the dynamic compliance. Note that the compliance in the z direction is not designed to decrease much, but its considerable decrease is also confirmed from the measured results and is thought to be caused mainly by damping within the press device.

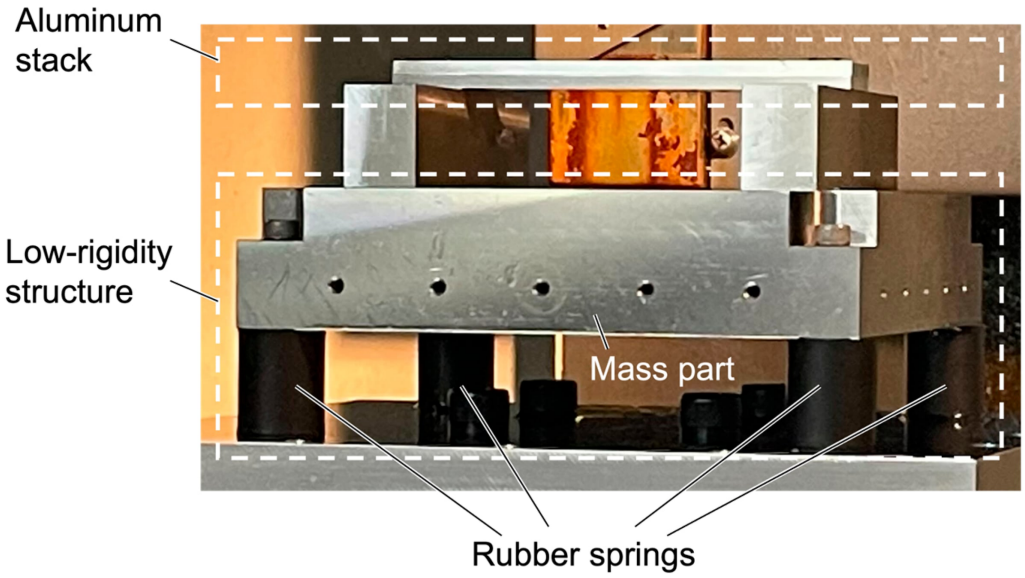


Figure 3. Photograph of a low-rigidity structure imitating aircraft assembly (the compliance of the robot is imitated in this paper).

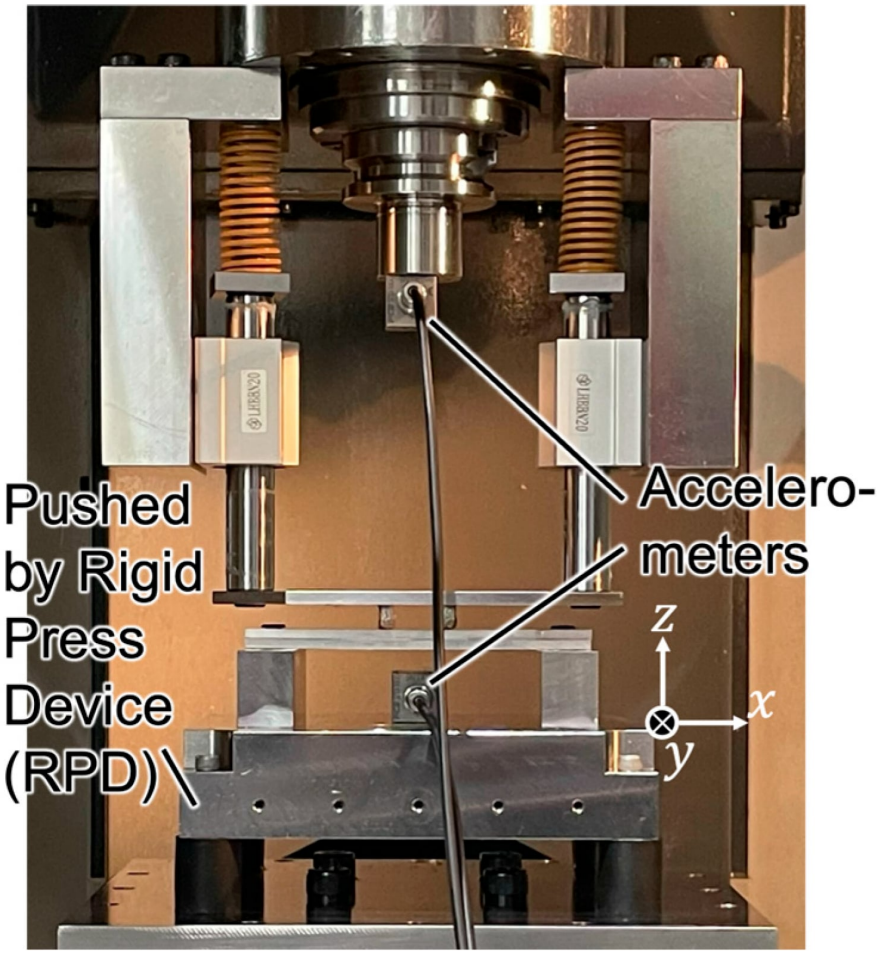


Figure 4. Photograph of hammering test setup with pressing by the proposed RPD.

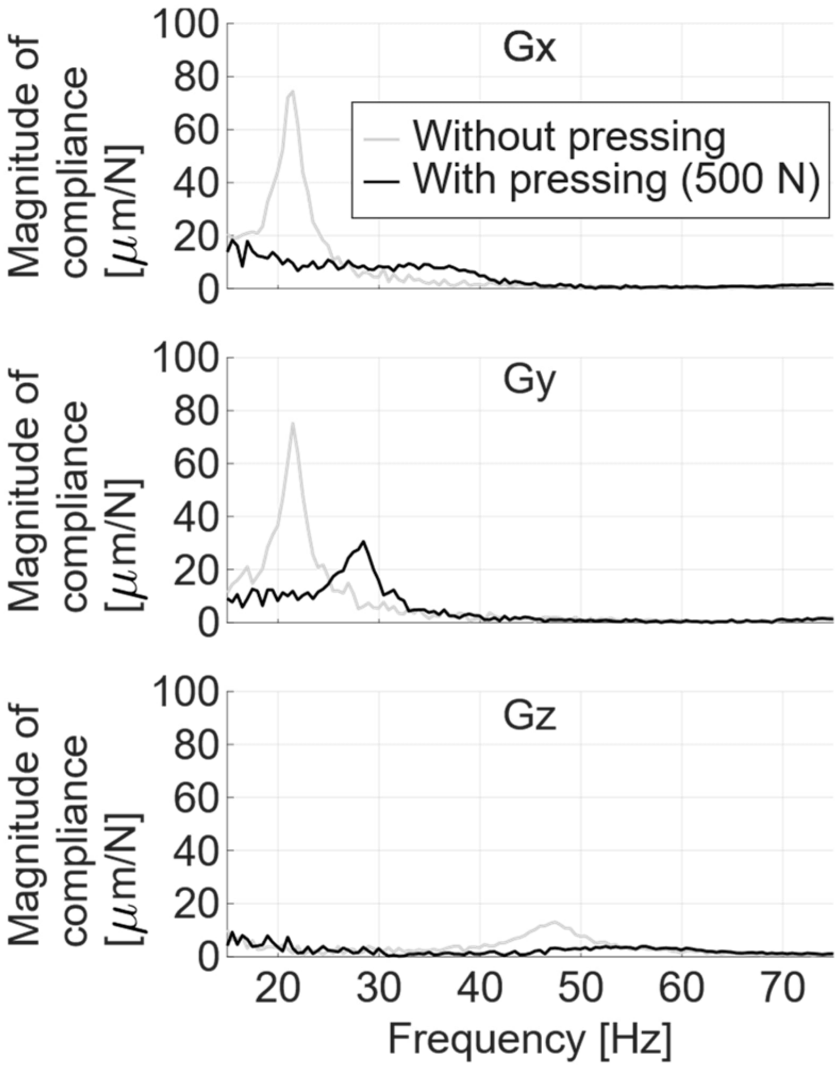


Figure 5. Direct components of measured loop compliance.

Table 1. Identified modal parameters.

Modal Parameters	Without Pressing	With Pressing
Mass [kg]	7.936 (*x* dir.)	13.720 (*x* dir.)
	7.859 (*y* dir.)	9.704 (*y* dir.)
	9.090 (*z* dir.)	16.184 (*z* dir.)
Damping ratio [%]	4.651 (*x* dir.)	8.207 (*x* dir.)
	4.651 (*y* dir.)	5.263 (*y* dir.)
	4.737 (*z* dir.)	8.628 (*z* dir.)
Spring constant [kN/m]	144.532 (*x* dir.)	695.680 (*x* dir.)
	143.137 (*y* dir.)	310.558 (*y* dir.)
	808.033 (*z* dir.)	1938.545 (*z* dir.)

3. Experimental Investigation into Interlayer Gap and Low-Rigidity Problems

Drilling experiments are conducted to verify the proposed method. A photograph of the experiment is shown in Figure 6. In this paper, an aluminum (AlZn5.5MgCu, ISO) stack of two plates is chosen for the target, and they are machined on a 3-axis machining center (MILLAC415V, Okuma Corp (Oguchi, Japan)). As shown in the figure, it can be assumed that the initial gap is negligible. The force during pressing/cutting is measured

by a dynamometer (9255C, Kistler Instrumente AG (Winterthur, Switzerland)), and an accelerometer (356A01, PCB Piezotronics, Inc.) is set on the low-rigidity structure to measure the vibration during the experiments. Drilling with and without the press device is conducted, and the interlayer chip, vibration, and hole diameter are evaluated. The drilling conditions are shown in Table 2. The experiments are conducted three times for each condition (without and with pressing), and the representative results are shown in this paper, as all results are nearly the same; the suppression of vibration and interlayer chips and an increase in hole accuracy, caused by the RPD, are observed in all of the conditions. Note that since the uncut chip thickness decreases by the pressing, the set feed rate for the experiment with pressing is adjusted (increased) so that the thrust force due to drilling is nearly the same as that without pressing. This means that the proposed method should still be effective under the same set feed rate as that without pressing because the drilling thrust force should be lower, that is, the interlayer gap is zero or smaller.

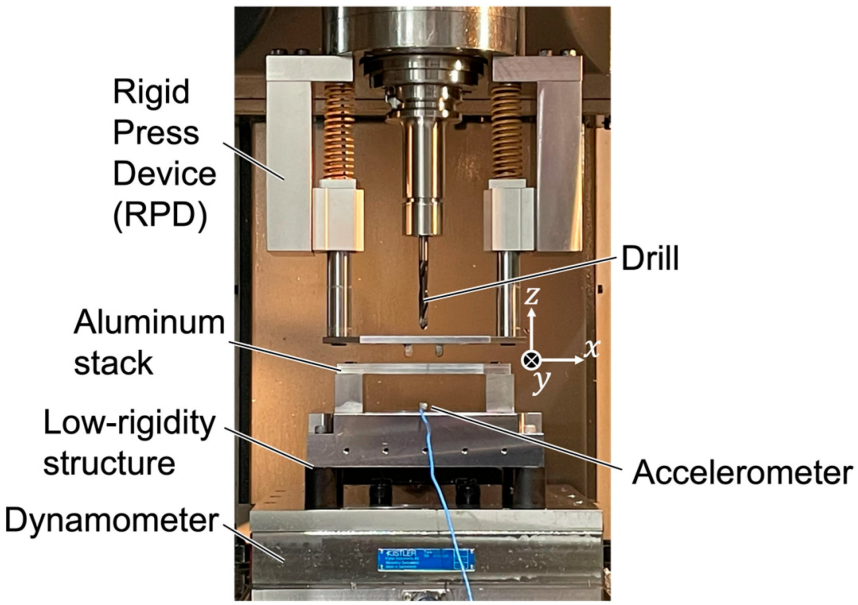


Figure 6. Photograph of drilling experiment.

Table 2. Drilling conditions.

Workpiece material	AlZn5.5MgCu (ISO)
Workpiece thickness	4 mm (top)/4 mm (bottom)
Tool material	DLC-coated carbide (2 flutes) (DLC-NF-GDN 8, OSG Corp (Toyokawa, Japan).)
Tool diameter	8 mm
Number of flutes	2
Spindle speed (Cutting speed)	2000 min^{-1} (50 m/min at outer diameter)
Set feed rate per tooth	0.025 mm/tooth (for without pressing) 0.04 mm/tooth (for with pressing)
Cutting fluid condition	Dry

First, the interlayer chips are evaluated. The measured force is shown in Figure 7. Note that the drill bites the free side of the top plate when exiting it, resulting in force/vibration and hole accuracy decrease in the ordinary drilling, whereas they are suppressed in the proposed RPD-drilling. Compared with ordinary robotic drilling, an additional force is observed with the proposed press device. In Figure 7b, the pressing force is subtracted

from the total force by utilizing the spring constant of the springs composing the RPD (or simply by fitting the ramp function in the figure) and the instant at which pressing begins. The latter can be detected from the graph. It can be observed that the pressing force is approximately 600 N when drilling into the bottom plate, whereas the drilling thrust force is approximately 500 N; the top plate is pressed sufficiently that the interlayer gap is eliminated/minimized. Note that the fluctuation of the thrust force is small, and it can be observed that a pressing force of 600 N is sufficient to suppress the gap. Note also that the thrust force with the elimination of the pressing force in the proposed method, as shown in Figure 7a, is slightly larger than that in the ordinary drilling setup; nevertheless, the proposed method is successful in suppressing the various problems discussed hereafter. Figure 8 shows photographs of the free/interlayer sides of the plates. As shown in Figure 8a, chips can be observed on the interlayer sides of the plates with ordinary robotic drilling. On the other hand, the interlayer chips cannot be observed in the proposed RPD-drilling, as shown in Figure 8b. This suggests that there is no or only a minimal interlayer gap when sufficient pressing force is applied. Note that the height color maps of all photographs are examined, confirming that interlayer chips are only observed in the ordinary robotic (imitated) drilling.

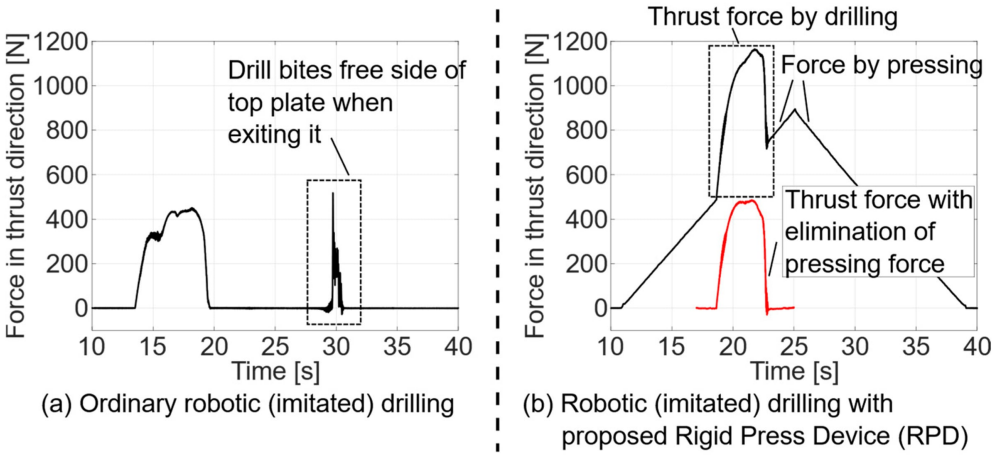


Figure 7. Example of measured forces.

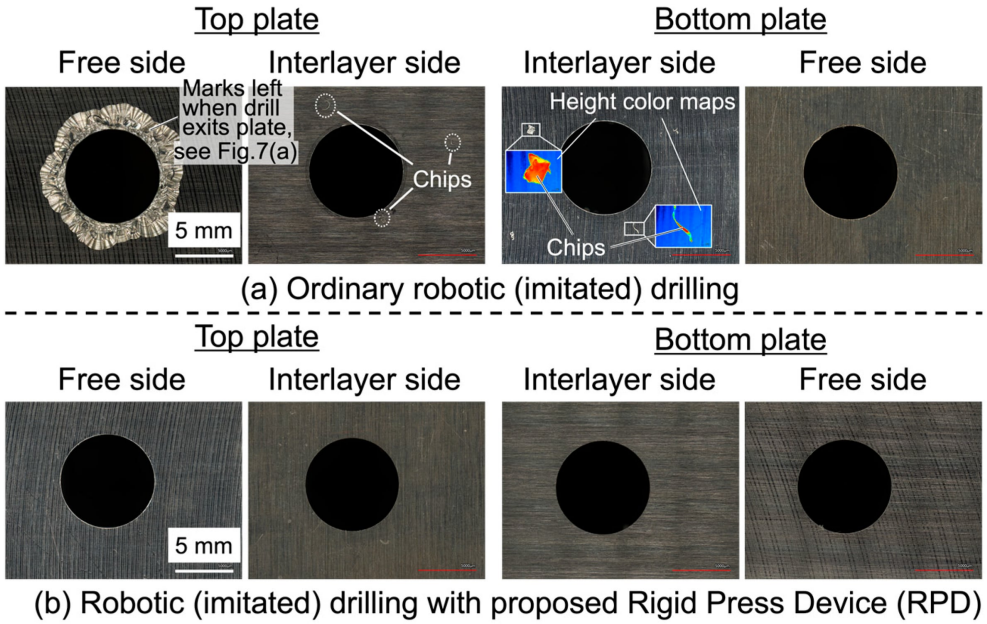


Figure 8. Photographs of plates after drilling.

Second, the vibration is evaluated. Figure 9 shows the measured vibration acceleration, and Figure 10 shows the short-time Fourier transform results of the vibration displacement during the drilling. Chatter in drilling can occur in any (*xyz*) direction as mentioned in for example [25]. As can be observed from the acceleration, large chatter vibration occurs at the beginning of the ordinary robotic drilling. For example, the root mean square value of the vibration acceleration shown in Figure 9 in the *x* direction during the drilling period in ordinary drilling is 8.35 m/s^2, whereas that in the proposed drilling method is 1.74 m/s^2; the vibration is greatly reduced. In fact, a displacement of over 870 μm is measured at a frequency of 27 Hz, which is slightly above the natural frequencies of the primary vibration modes in the *x* and *y* directions of the robot-imitated structure, as shown in Figure 5. In addition, forced vibration of over 65 μm can be observed at the spindle-speed frequency (33.3 Hz) near the end of drilling. On the other hand, chatter is suppressed, and only smaller forced vibration of about 15 μm can be observed in the proposed RPD-drilling in this representative case. This means that chatter and forced vibrations can be suppressed effectively owing to the high rigidity of the proposed RPD.

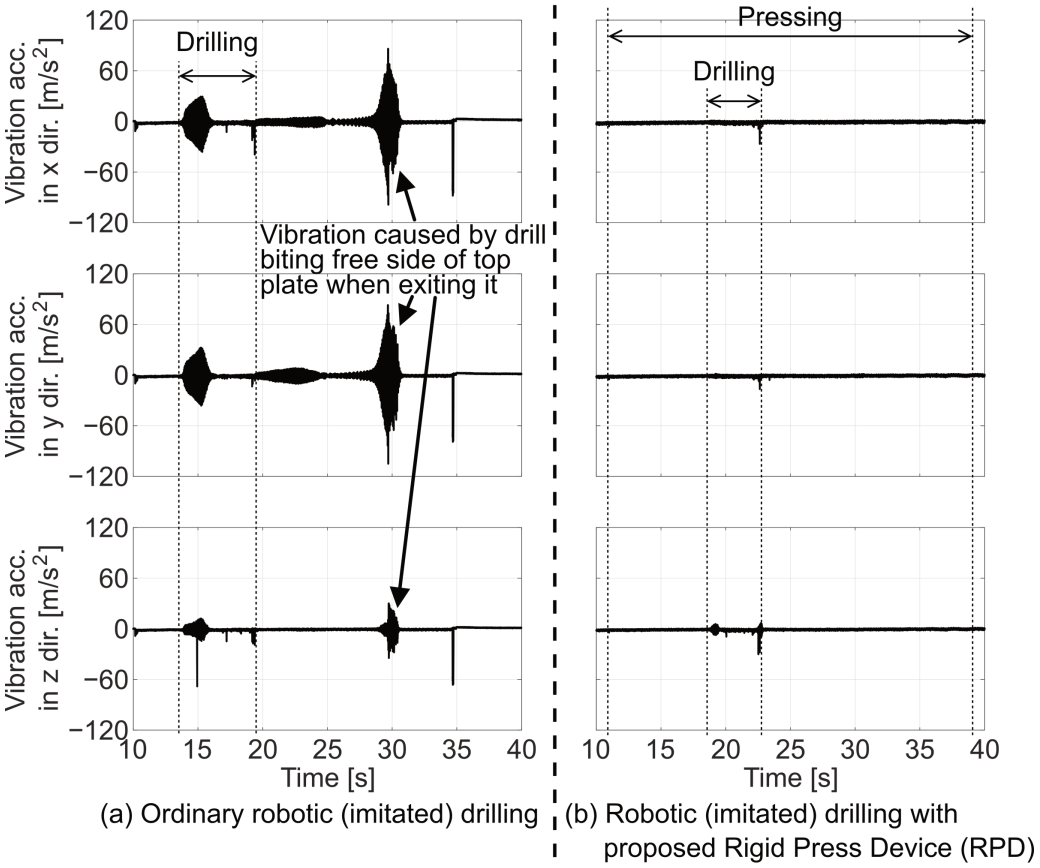


Figure 9. Example of measured vibration acceleration.

Finally, the hole diameter is evaluated. The hole diameter measured by a CNC coordinate measuring machine (CRYSTA-Apex V574, Mitutoyo Corp (Kawasaki, Japan)) is shown in Figure 11. Two results are shown for each condition (without and with pressing). Note that the hole diameter near the free side of the top plate is not evaluated since its decrease is obvious, and that of the inside of the hole is evaluated. It can be observed that the hole diameter without pressing is larger than that with pressing. Moreover, the hole diameter in the top plate without pressing is large, and this is mainly because of the chatter vibration that occurred at the beginning of ordinary robotic drilling.

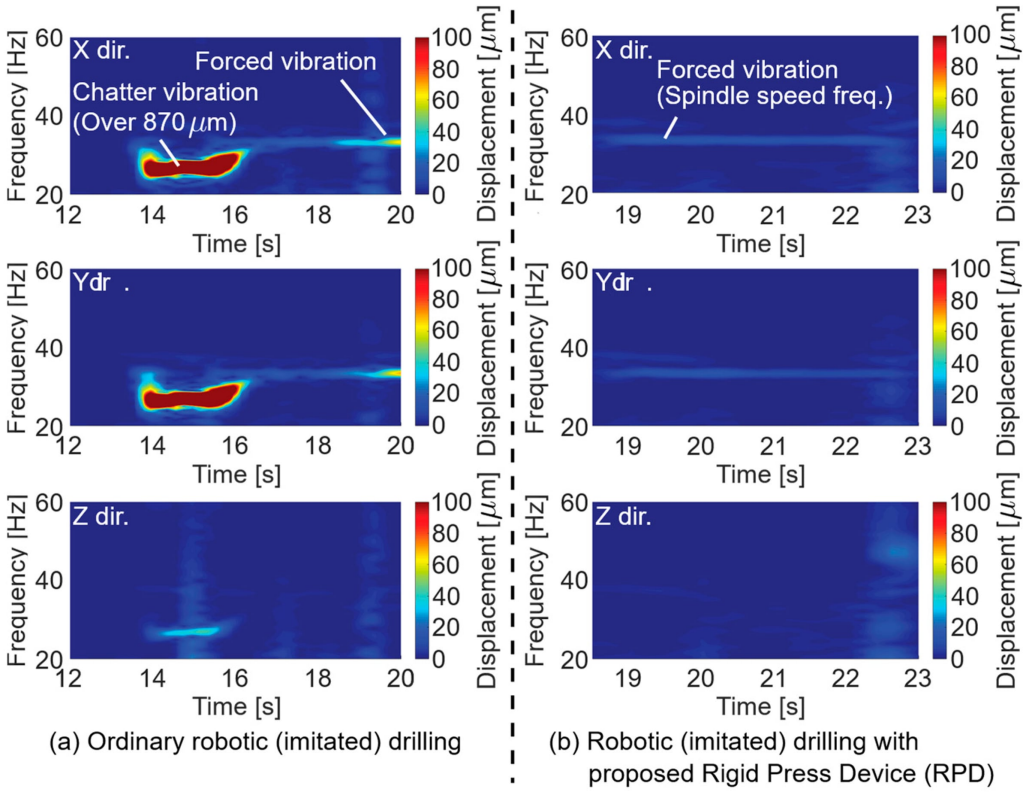


Figure 10. Short-time Fourier transform results of measured vibration displacement during drilling.

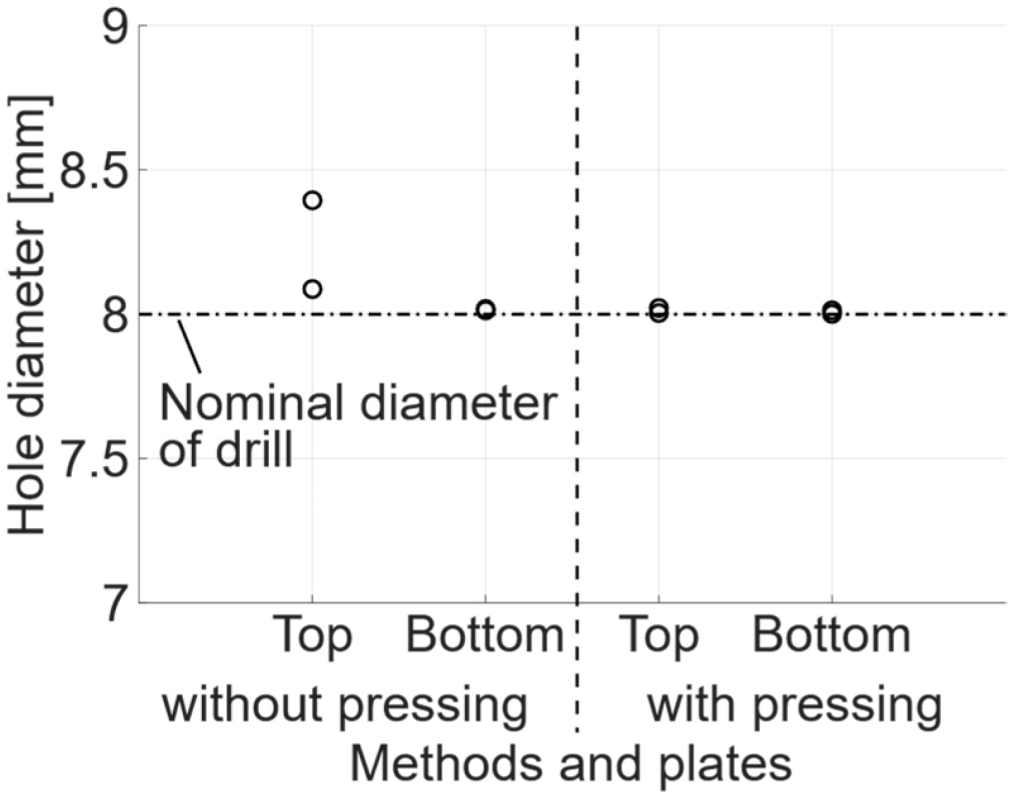


Figure 11. Measured hole diameter.

From these results, it can be concluded that the proposed method is effective for robotic stack drilling.

4. Conclusions

A Rigid Press Device (RPD) was developed in this paper to solve problems that occur in robotic stack drilling. To solve the interlayer gap problem, passive pressing is applied by springs so that the interlayer gap is eliminated by a simple structure. To solve the low-rigidity problem, the press device was designed in a compact and rigid form so that a small closed compliance loop is formed when pressing is applied. Owing to this small loop, the static/dynamic compliance of the machining system decreases greatly even though the system includes the low-rigidity robot and thin plates. Its rigidity-increasing effect was confirmed through hammering tests of a robot-imitating compliant structure, where a maximum decrease of 88% in dynamic compliance was observed. Drilling experiments were conducted on a two-layer aluminum stack mounted on a robot-imitating compliant structure, whose compliance is similar to that of industrial robots in terms of magnitude, resonance, and damping. It was suggested based on interlayer chip observations that the interlayer gap was suppressed; no interlayer chips were observed when drilling with the proposed RPD. In addition, vibration problems were suppressed when the proposed RPD-drilling is utilized, and the hole diameter accuracy was also improved. Therefore, it can be concluded that the developed RPD has the potential to be applied in robotic stack drilling in aircraft assembly, which will be investigated in future work. In particular, research will focus on technical points, such as optimization of RPD structure so that the proposed method meets the robot payload requirements, enhancement of the RPD for further improvement of dynamic characteristics, and application to curved surfaces (e.g., the aircraft skin), among others.

Author Contributions: Conceptualization, T.H. and E.S.; methodology, T.H., R.S. and E.S.; software, R.S.; validation, T.H., R.S. and E.S.; formal analysis, T.H., R.S., K.L. and E.S.; investigation, T.H., R.S. and E.S.; resources, T.H. and E.S.; data curation, T.H. and R.S.; writing—original draft preparation, T.H.; writing—review and editing, T.H., R.S. and E.S.; visualization, T.H. and E.S.; supervision, T.H., K.L., and E.S.; project administration, T.H. and E.S.; funding acquisition, T.H. and E.S. All authors have read and agreed to the published version of the manuscript.

Funding: This research was funded by the Human Resource Development and Research Project on Production Technology for the Aerospace Industry: a Subsidy from Gifu Prefecture.

Data Availability Statement: The original contributions presented in this study are included in the article. Further inquiries can be directed to the corresponding author.

Acknowledgments: The authors would like to express their sincere thanks to the engineers of Kawasaki Heavy Industries, Ltd. for their assistance in conducting the present research.

Conflicts of Interest: The authors declare no conflicts of interest.

Abbreviations

The following abbreviations are used in this manuscript:

RPD	Rigid Press Device
RPD-drilling	Drilling with the Rigid Press Device

References

1. Verl, A.; Valente, A.; Melkote, S.; Brecher, C.; Ozturk, E.; Tunc, L.T. Robots in machining. *CIRP Ann.–Manuf. Technol.* **2019**, *68*, 799–822. [CrossRef]
2. Ji, W.; Wang, L. Industrial robotic machining: A review. *Int. J. Adv. Manuf. Technol.* **2019**, *103*, 1239–1255. [CrossRef]
3. Wang, W.; Guo, Q.; Yang, Z.; Jiang, Y.; Xu, J. A state-of-the-art review on robotic milling of complex parts with high efficiency and precision. *Robot. Comput.-Integr. Manuf.* **2023**, *79*, 102436. [CrossRef]
4. Cordes, M.; Hintze, W.; Altintas, Y. Chatter stability in robotic milling. *Robot. Comput.-Integr. Manuf.* **2019**, *55*, 11–18. [CrossRef]

5. Garnier, S.; Subrin, K.; Waiyagan, K. Modelling of robotic drilling. *Procedia CIRP* **2017**, *58*, 416–421. [CrossRef]
6. Zaeh, M.F.; Schnoes, F.; Obst, B.; Hartmann, D. Combined offline simulation and online adaptation approach for the accuracy improvement of milling robots. *CIRP Ann.–Manuf. Technol.* **2020**, *69*, 337–340. [CrossRef]
7. Jin, Y.; Gu, Q.; Liu, S.; Yang, C. Experimental investigation and modeling of force-induced surface errors for the robot-assisted milling process. *Machines* **2023**, *11*, 655. [CrossRef]
8. The Boeing Company. 777 Quality Information. Available online: https://www.boeing.com/commercial/777/quality-information (accessed on 16 September 2026).
9. Tamura, J. Aviation and Space (Process & Construction). *J. Jpn. Weld. Soc.* **2014**, *83*, 209–214. (In Japanese) [CrossRef]
10. Hassan, A.A.; Soo, S.L.; Aspinwall, D.K.; Arnold, D.; Dowson, A. An analytical model to predict interlayer burr size following drilling of CFRP-metallic stack assemblies. *CIRP Ann.–Manuf. Technol.* **2020**, *69*, 109–112. [CrossRef]
11. Luo, B.; Zhang, K.; Liu, S.; Cheng, H.; Wang, R. Investigation on the interface damage in drilling low-stiffness CFRP/Ti stacks. *Chin. J. Aeronaut.* **2019**, *32*, 2211–2221. [CrossRef]
12. Tunc, L.T.; Gonul, B. Effect of quasi-static motion on the dynamics and stability of robotic milling. *CIRP Ann.–Manuf. Technol.* **2021**, *70*, 305–308. [CrossRef]
13. Guo, Y.; Dong, H.; Ke, Y. Stiffness-oriented posture optimization in robotic machining applications. *Robot. Comput.-Integr. Manuf.* **2015**, *35*, 69–76. [CrossRef]
14. Qiu, X.Y.; Yu, Z.; Li, C.P.; Niu, Q.L.; Li, S.J.; Li, P.N.; Ko, T.J. Influence of main cutting edge structure on hole defects in CFRP/titanium alloy stacks drilling. *J. Manuf. Process.* **2021**, *69*, 503–513. [CrossRef]
15. Zhu, Z.; Guo, K.; Sun, J.; Li, J.; Liu, Y.; Zheng, Y.; Chen, L. Evaluation of novel tool geometries in dry drilling aluminum 2024-T351/titanium Ti6Al4V stack. *J. Mater. Process. Technol.* **2018**, *259*, 270–281. [CrossRef]
16. Hu, Y.; Song, Y.; Li, Y.; Yao, Z. An analytical model to predict interfacial burr height for metal stack drilling. *Proc. Inst. Mech. Eng. Part B J. Eng. Manuf.* **2019**, *233*, 99–108. [CrossRef]
17. Lei, C.; Li, C.; Bi, Y.; Li, J. The optimal clamping force option for robotic drilling of stacked aluminum sheets based on shell theory. *Adv. Mech. Eng.* **2017**, *9*, 1–9. [CrossRef]
18. Olsson, T.; Haage, M.; Kihlman, H.; Johansson, R.; Nilsson, K.; Robertsson, A.; Björkman, M.; Isaksson, R.; Ossbahr, G.; Brogårdh, T. Cost-efficient drilling using industrial robots with high-bandwidth force feedback. *Robot. Comput.-Integr. Manuf.* **2010**, *26*, 24–38. [CrossRef]
19. Liang, J.; Bi, S. Design and experimental study of an end effector for robotic drilling. *Int. J. Adv. Manuf. Technol.* **2010**, *50*, 399–407. [CrossRef]
20. Kazemiesfahani, M.; Dilfanian, E.; Monsarrat, B.; Hajzargarbashi, S. Design, Analysis, and Prototyping of a Multifunctional Digital Twin-Enabled Aerospace Drilling End-Effector Deployable by a Collaborative Robot. *Sensors* **2025**, *25*, 7504. [CrossRef] [PubMed]
21. Zheng, X.; Zhang, G.; Zhou, C.; Guo, G. Hole diameter deviation control method for robotic hole-making system based on presser foot action. *Int. J. Precis. Eng. Manuf.* **2024**, *25*, 319–333. [CrossRef]
22. Mei, B.; Zhu, W. Accurate positioning of a drilling and riveting cell for aircraft assembly. *Robot. Comput.-Integr. Manuf.* **2021**, *69*, 102112. [CrossRef]
23. Zhang, J.; Liao, W.; Bu, Y.; Tian, W.; Hu, J. Stiffness properties analysis and enhancement in robotic drilling application. *Int. J. Adv. Manuf. Technol.* **2020**, *106*, 5539–5558. [CrossRef]
24. Huynh, H.N.; Assadi, H.; Rivière-Lorphèvre, E.; Verlinden, O.; Ahmadi, K. Modelling the dynamics of industrial robots for milling operations. *Robot. Comput.-Integr. Manuf.* **2020**, *61*, 101852. [CrossRef]
25. Altintas, Y.; Weck, M. Chatter stability of metal cutting and grinding. *CIRP Ann.* **2004**, *53*, 619–642. [CrossRef]

Disclaimer/Publisher's Note: The statements, opinions and data contained in all publications are solely those of the individual author(s) and contributor(s) and not of MDPI and/or the editor(s). MDPI and/or the editor(s) disclaim responsibility for any injury to people or property resulting from any ideas, methods, instructions or products referred to in the content.